Journal of Materials Chemistry A

ROYAL SOCIETY OF CHEMISTRY

PAPER

View Article Online
View Journal

Cite this: DOI: 10.1039/d0ta05337f

Interfacial self-assembled GR/GO ultrathin membranes on a large scale for molecular sieving†

Junyuan Xia,[ab] Peng Xiao,[a] Jincui Gu,*[ab] Tianyu Chen,[a] Chaohui Liu,[c] Luke Yan*[c] and Tao Chen*[abc]

Graphene oxide (GO) has superior molecular sieving abilities due to its unimpeded two-dimensional (2D) nano-channels and nacre-like lamellar structure. However, it remains a huge challenge to fully exploit its unmatched features to construct a GO-based membrane on a large scale for excellent screening performance. Here, we display a facile, ultrafast and environmentally friendly strategy to design an ultrathin (graphene/graphene oxide@polyetherimide) GR/GO@PEI composite membrane under the collective effects of a hydrophilic PEI molecular-bridge and an ordered GR/GO laminar structure. Excitingly, this composite membrane presents extraordinary structural stability, even when transferred to any given substrate, regardless of its chemical components, structure, or specification. Furthermore, this membrane shows high permeance of up to 191 L m^{-2} h^{-1} bar^{-1} and over 99% rejection of Congo red, far superior to the majority of GO-based separation membranes reported so far. In addition, it can withstand several types of physical damage and chemical corrosion, as well as being further able to realize the purification of actual, complex, multi-component, domestic sewage. This work will open the door to developing scalable 2D lamellar membranes with ultrafast and precise separation channels for practical water purification.

Received 26th May 2020
Accepted 9th August 2020

DOI: 10.1039/d0ta05337f

rsc.li/materials-a

1. Introduction

Water is the source of life. The purification of molecules at the nanometre scale is one of the most significant and intractable tasks concerned with the ecological environment.[1–3] Membrane separation materials have attracted intense attention for sustainable water purification on a universal scale since they are energy efficient, environmentally benign and have low energy consumption.[4–6] Currently, the majority of separation membranes are polymer-based or ceramic-based materials. In spite of this, several shortcomings, such as low permeation flux, poor chemical resistance and weak anti-fouling ability, have restrained their further development.[7,8] Therefore, advanced separation membranes which are capable of running in an extensive range of operating conditions with outstanding permeation and rejection, are urgently required.

To date, scientists have made considerable efforts to establish two-dimensional (2D) next-generation membranes, such as g-C_3N_4,[9,10] MXenes,[11,12] molybdenum disulfide (MoS_2) nanosheets,[13,14] covalent organic frameworks (COFs),[15–18] and metal–organic framework (MOF) nanosheets.[19–21] These 2D membranes, presented in the form of single layers, multi-layered stacks or a uniformly mixed matrix, have featured distinct superiorities of adjustable interlayer space and chemical structure, ultrafast molecular permeability, precise sieving and chemical stability.[21] Therefore, plentiful achievements have been made in this newly established field. In particular, graphene oxide (GO), with an expanded lateral dimension and nano-scale thickness, has generated enormous interest from the science field to explore its transport behaviour and mechanism.[22,23] On the one hand, it has a huge specific surface area and hydrophilic functional groups (such as hydroxy and carboxyl), promoting it as an optimal choice to realize highly-efficient interfacial contact with the water-soluble components.[24] On the other hand, it can be designed with a shell-like continuous architecture by interpenetrating, crosslinking or self-assembly, which is beneficial for capturing the target molecules.[25] So far, numerous exciting breakthroughs in GO-based membranes in separation science have sprung up.[26–32] For instance, Wu *et al.* have reported a GO-based composite membrane by intercalating it with (titanium dioxide) TiO_2 nanoparticles through the oxidation of MXene nanosheets.[33] The consecutively distributed TiO_2 nanocrystals can create

[a]Key Laboratory of Marine Materials and Related Technologies, Zhejiang Key Laboratory of Marine Materials and Protective Technologies, Ningbo Institute of Material Technology and Engineering, Chinese Academy of Science, Ningbo 315201, China. E-mail: gujincui@nimte.ac.cn; tao.chen@nimte.ac.cn

[b]School of Chemical Sciences, University of Chinese Academy of Science, Beijing 100049, China

[c]Polymer Materials & Engineering Department, School of Materials Science & Engineering, Chang'an University, Xi'an 710064, China. E-mail: yanlk_79@hotmail.com

† Electronic supplementary information (ESI) available: Additional characterization and measurement results. See DOI: 10.1039/d0ta05337f

additional channels for water permeation. Therefore, this membrane has shown a high water flux of 89.6 L m^{-2} h^{-1} bar^{-1} and excellent dye rejection ability (over 97%). Wang and co-workers have developed a GO-based membrane with intersecting channels by *in situ* alternating dispersed sub-5 nm silica nanoparticles into the interlayers of GO.[34] These nanoparticles assumed the role of spacers to tune the physical and chemical microenvironment to endow the GO membrane with fast solvent transport and high rejection of small molecules. Therefore, this composite membrane has exhibited excellent rejection of dyes (90%) with sizes over 1.5 nm. Very recently, Chen *et al.* presented a 2D GO-based membrane by combining thin COF and partially reduced GO. The COF served as a support layer to broaden the interlayer spacing between the GO nanosheets, which endowed this membrane with a high water throughput of 194 L m^{-2} h^{-1} bar^{-1} and 98% rejection ability for methyl blue.[35] Besides, other numerous attempts, such as cross-linking,[24,25,27,31] partial reduction,[36] and cationic control[32,37] have been undertaken to modulate the interlayer spacing of GO membranes for selective molecular separation. Despite these pioneering works, the majority of the designed GO-based membranes on substrates are produced by spin-casting, drop-casting, spraying or vacuum filtration.[38] How to fully utilize its unique features and develop a scalable GO-based membrane through a facile, ultrafast and environmentally friendly approach for superior permeability and molecular screening remains a challenge.

In our previous work, we presented series of polymer functionalized carbon nanotube (CNT)-based membranes through the interfacial self-assembly process.[39,40] The micromorphology and chemical composition can be well controlled by regulating the volume amount of CNTs dispersed as well as the types of polymers. Moreover, there were more hydrophilic groups (such as hydroxy and carboxyl) on the water side than on the air side in the self-assembled CNT membrane. By virtue of these merits, we report here for the first time the fabrication of a GO-based ultrathin membrane at large scale for efficient molecular sieving. Schematics of the fabrication process are shown in Fig. 1 and S1.† Firstly, the graphene (GR) ethanol dispersion was sprayed onto the GO dispersion on the air/water interface. Benefiting from the Marangoni force, the GR sheets rapidly extended from the ethanol-rich zones with low surface tension to the water-rich zones with high surface tension.[39] The π stacking and the hydrogen bond force between GR and GO further facilitated the formation of a GR/GO layer on the water surface (Fig. 1A and S1A†).[41–43] Furthermore, owing to the amphiphilicity of GO, they tend to move toward the air/water interface to reduce the surface tension of the liquid phase.[44] Secondly, a porous sponge was used to compress the GR/GO membrane from a loose state to a compact mode at the air/

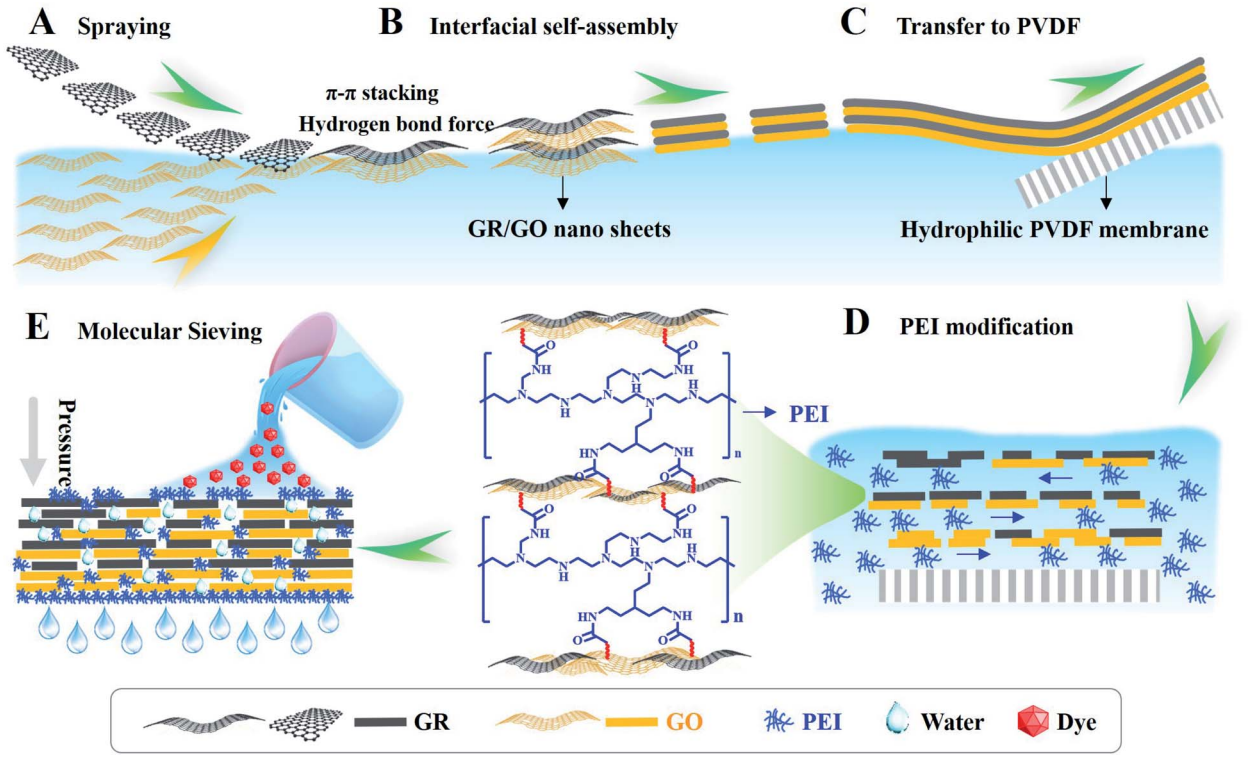

Fig. 1 A schematic illustration of the construction of the GR/GO@PEI composite membrane through a self-assembly process at the air/water interface and its application to molecular sieving. (A) A GR ethanol dispersion was evenly sprayed onto the air/GO dispersion interface. In this process, π–π stacking and hydrogen bond forces between GR and GO promoted the formation of a GR/GO layer at the water surface. (B) A porous sponge was applied to compress the GR/GO membrane from a loose mode to a closely packed state on the air/water surface. (C) The GR/GO membrane was transferred in parallel onto a PVDF substance pre-treated with plasma. (D) The GR/GO membrane was immersed in PEI solution. In this process, PEI served as a molecular bridge through forming strong covalent bonds with the GR/GO nanosheets. (E) The obtained GR/GO@PEI composite membrane was further applied to the purification of wastewater.

water surface (Fig. 1B and S1B†). Subsequently, the GR/GO membrane was transferred in parallel to a commercial (polyvinylidene fluoride) PVDF substance (Fig. 1C). Lastly, it was immersed in the polyetherimide (PEI) solution and the GR/GO@PEI composite membrane was obtained (Fig. 1D and S1C†). Importantly, the interfacial long-chain PEI molecular bridge and the interlocked layered structure endowed the GR/GO@PEI composite membrane with ultrathin thickness and excellent mechanical strength and flexibility, which can be transferred to any substance regardless of its chemical components, structure or specification. Furthermore, the hydrophilic PEI can preferentially capture plenty of water molecules, resulting in an increase in the driving force across the GR/GO membrane (Fig. 1E). Therefore, the GR/GO@PEI composite membrane can separate various dye molecules in a fast manner with a maximum permeation of up to 191 L m^{-2} h^{-1} bar^{-1} and over 99% rejection for Congo red, which exceeds that of the majority of GO-based separation membranes previously reported. In addition, with the rational design of the molecular bridges, this composite membrane has exhibited outstanding physical and chemical durability under several types of damage or harsh conditions, including strong acidic and alkaline aqueous solutions. This work will open up a new avenue for the construction of scalable GO-based separation membranes through an ultrafast and environmentally friendly strategy for applications in water-related purification.

2. Experimental

2.1 Materials

Graphene oxide (GO) powder was obtained from Nanjing JCNANO Technology Co., Ltd *via* a modified Hummer's method. Graphene (GR) was obtained from Ningbo Morsh Technology Co., Ltd. Polyethyleneimines (PEI) with different molecular weights (600, 1800, 10 000, 70 000) were provided by Aladdin (Shanghai) Co., Ltd. Polyvinylidene fluoride (PVDF) filter paper (aperture 0.22 μm) was obtained from Millipore Industrial & Lab Chemicals. Ceramic tubes, titanium plates and alumina ceramic sheets were bought from Wuxi Teke Fine Ceramics Co., Ltd. Different anionic dye molecules, including: Evans blue (EB, 960.8 g mol^{-1}), methyl blue (MB, 799.8 g mol^{-1}), Congo red (CR, 696.6 g mol^{-1}), eriochrome black T (EBT, 461.3 g mol^{-1}), cresol red sodium salt (CSS, 404.4 g mol^{-1}), methyl orange (MO, 327.3 g mol^{-1}), as well as different cationic dye molecules, including: victoria blue B (VBB, 506.08 g mol^{-1}), rhodamine B (Rh. B, 479.01 g mol^{-1}), methyl violet (MV 407.99 g mol^{-1}), and *N*,*N*-dimethyl-*p*-phenylenediamine dihydrochloride (DMPD, 209.12 g mol^{-1}) were provided by Sigma-Aldrich Co., Ltd. All the other chemicals were received from J&K Scientific Co. Ltd.

2.2 Fabrication of a GR/GO@PEI composite membrane

Firstly, the GR ethanol dispersions (1 mg mL^{-1}) were prepared by sonication for 30 min under 400 Hz. Secondly, 25 mL of GR ethanol dispersion was sprayed onto the air/GO dispersion interface. The concentration of the GO dispersion was 0.05–0.5 mg mL^{-1}. Thirdly, after aging for 1 h under 25 °C, a porous sponge was used to compress the GR/GO layer from one side. Lastly, the GR/GO membrane was shifted to the PVDF substrate which had been pre-treated with oxygen plasma for 60 s, and then immersed in PEI (5 mg mL^{-1}, 10 mL) solution for 30 min. The molecular weights of the PEI were 600 g mol^{-1}, 1800 g mol^{-1}, 10 000 g mol^{-1}, 70 000 g mol^{-1}, respectively. The GR/GO@PEI composite membrane was dried in a vacuum oven under 60 °C for 1 h. The mass ratio of the GR and GO in the GR/GO membrane was about 3 : 1 (Fig. S2†).

2.3 Rejection performance of the GR/GO@PEI composite membrane

To simulate an industrial membrane filtration process, the permeation process was implemented upon a homemade cross-flow filtration apparatus with an effective filtration area of 6.15 cm^2. The separation flux was evaluated by measuring the filtration volume after 1 h under a pressure of 1 bar.

The separation flux J was calculated according to the equation:

$$J = V/(S \times T) \quad (1)$$

where V (L) is the filtrate volume, S (m^2) is the filtration area, and T (h) is the permeation time.

The separation efficiency was tested by the formula below:

$$R = (1 - C_a/C_o) \times 100\% \quad (2)$$

where C_o and C_a are the concentrations of dye molecules in the feed and filtration, respectively.

2.4 Characterization

The morphological images of the membranes were obtained with scanning electronic microscopy, SEM (Hitachi S4800, Japan), transmission electronic microscopy, TEM (JEOL2100 HR, America) and laser scanning confocal microscopy, LSCM (LSM 800, Germany). The cross-sectional images of the membranes were recorded on the TEM (JEOL2100 HR, America) and Focused Ion Beam, FIB (Helios-G4-CX, America). The wettability of the membrane was performed on a contact angle measuring instrument (OCA-20, America) at room temperature. The chemical constituent of each sample was investigated by X-ray photoelectron spectroscopy, XPS (Shimadzu Axis Untraded spectroscope, Japan). The chemical bonds were characterized by an infrared spectrometer, IR (Nicolet 6700, America). The interlayer spacing of each membrane was tested with an X-ray diffractometer, XRD (D8 Discover, Germany). The distribution of the elemental composition for the composite membrane was further tested by etching the membrane surface with a step length of 20 nm to the interior at a depth of up to 200 nm. Raman spectroscopy was also carried out on a Via-reflex spectrometer (England) using 514 nm wavelength incident laser light in the range from 5000 to 3000 cm. Zeta potentials were obtained with a zeta potential analyser (Nano ZS, England). The molecular concentrations of the feed and filtration were analysed using an ultraviolet-visible spectrophotometer, UV-vis (Lambda 950, Japan). The thermal degradation process of the

membrane was evaluated by thermogravimetric analysis, TGA (PerkinElmer STA600, America).

3. Results and discussion

3.1 Membrane structure

The interfacial self-assembly process of this free-standing GR/GO membrane is shown in Fig. S3.† A homogeneous GR/GO thin membrane in a loose state was formed after the GR ethanol dispersion was sprayed onto the air/GO solution surface (Fig. S3B†). However, under the inducement of a porous sponge with plentiful capillary pores, this incompact mode was changed into a close form and a free-standing GR/GO membrane was finally achieved (Fig. S3C†). With strong connections, the GR/GO membrane was able to maintain this state even if the sponge was withdrawn. Interestingly, the macro-size of this GR/GO membrane can be regulated by controlling only the container and the amount of GR dispersed (Fig. S3†, 2A and B). Furthermore, the free-standing GR/GO membrane could be transferred to arbitrary target substrates even if they had different shapes, sizes or chemical compositions (Fig. S4†). Surprisingly, this GR/GO membrane can be also be distributed with high uniformity on a flat PVDF filter substance with a porous structure (Fig. S5†) on a large-area scale (Fig. 2C).

The surface topographies of GO and GR can affect the lamellar structure of the GR/GO@PEI composite membrane. GO presents a nearly transparent and ultrathin structure with many small, wave-like ripples (Fig. S6A†). HRTEM images presented a clear perspective of GO, which further demonstrated the uniformly folded structure in the GO sheet (Fig. 2D). The lateral dimension of the GR sheet was 4–8 μm (Fig. S6B†) and it had a multi-layer stacking structure (Fig. S6C and D†). There were some irregular wrinkles and protrusions in both the GR (Fig. S7A and C†) and GO (Fig. 2E, S7B and D†) membranes, which provided favourable transmission channels for water molecules.

The GR/GO membrane showed a wrinkled surface and stacking of multiple layers (Fig. S8A†). Interestingly, there was an obvious morphological difference between the two sides of the GR/GO membrane. The upper side (Fig. S9A and S10A†) was rougher than the lower side (Fig. S9B and S10B†). This asymmetric morphology indicated the uneven distribution of the GR in the GR/GO membrane (Fig. S8B†). However, after modification with PEI, the surface morphology of the GR/GO@PEI composite membrane became rougher (Fig. 2F and G). It was noteworthy that the lower side presented a smoother state (Fig. S9 and S10†), which indicated that the majority of PEI had formed covalent cross-linking with the GO sheets, whereas only a few of the PEI molecules had interacted with the GR sheets.

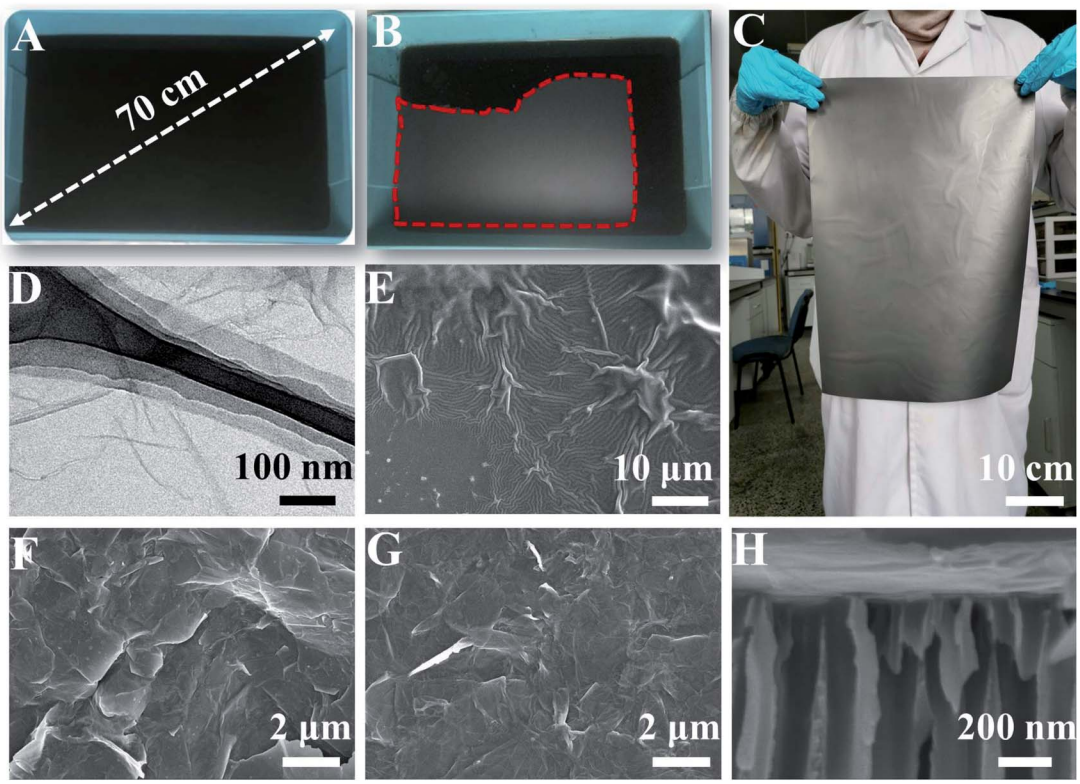

Fig. 2 Photographs of (A) GO solution and (B) the free-standing GR/GO membrane after the application of a porous sponge in a plastic container with a large area. In the process, the GR/GO membrane changed from a loose state into a close compacted state. (C) The GR/GO membrane was high-uniformly distributed on a flat PVDF filter substance on a large-area scale. (D) TEM and (E) SEM images of GO. SEM images of the upper side (F) and the lower side of the GR/GO@PEI composite membrane (G). (H) A cross-sectional SEM image of the GR/GO@PEI composite membrane, indicating its wrinkled surface and stacked multiple layered structure.

The cross-sectional morphology of the GR/GO@PEI composite membrane was further investigated by SEM and FIB. It can be clearly seen that the GR/GO@PEI composite membrane shows wrinkled surfaces and stacked multiple layer structures (Fig. 2H). Such a laminated structure could cause the defects in each individual sheet to be shielded by the neighbouring one, minimizing the ability of molecules to bypass the membrane interface. Furthermore, the GR membrane has a thin (~65.4 nm) and flat structure (Fig. 3A). However, the thickness of the GR/GO membrane increased to about 106 nm (Fig. 3B). In addition, there was almost no change in thickness even when the GR/GO membrane was modified with PEI (Fig. 3C).

3.2 Membrane wettability and chemical composition

To understand the interfacial self-assembly process more clearly, WCA measurements were taken to characterize the hydrophilicity of each membrane. As shown in Fig. 3D, S11, Movies S1 and S2,† there was about a 25° disparity between the upper and the lower sides of the GR membrane. This asymmetric wetting came from the uneven distribution of hydrophilic functional groups (such as carboxyl and hydroxyl) in the GR sheet.[39] Furthermore, the difference in WCA in the two sides of the GR/GO membrane increased to ~33° due to the π–π bond interaction and hydrogen bonding force between GR and GO (Movies S3 and S4†). These results further proved the asymmetry of the GR/GO membrane, which was consistent with the SEM results. However, there was almost no change between the sides of the GR/GO@PEI composite membrane, which was attributed to the inter-laminar molecular bridge of hydrophilic PEI (Movies S5 and S6†). The zeta potentials of the GO solution and GR/GO solution were studied further. As displayed in Fig. S12,† the zeta potentials of the GO and GR/GO solutions were about −46.9 mV and −62.2 mV, respectively. These results

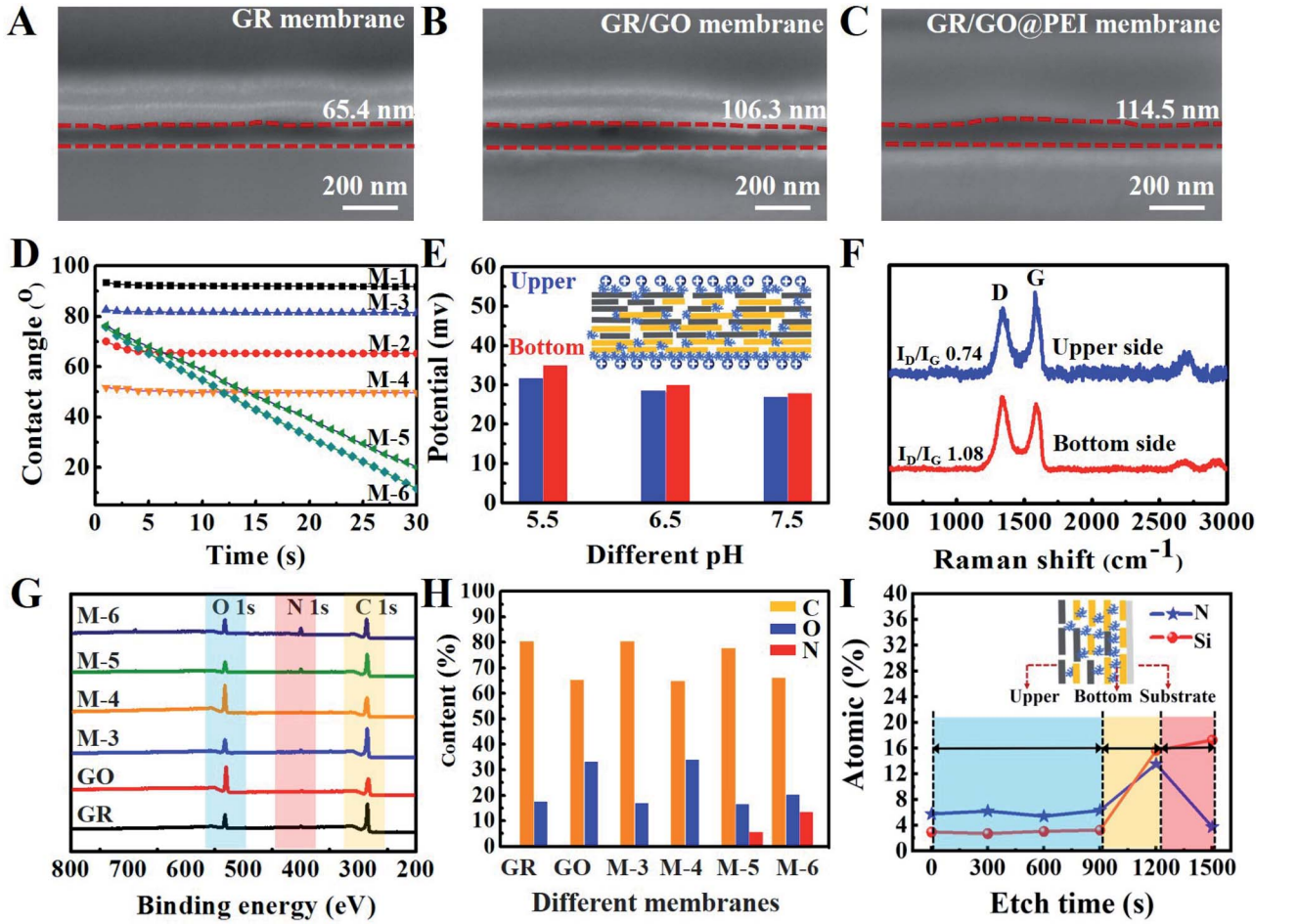

Fig. 3 Cross-sectional FIB images of the (A) GR membrane, (B) GR/GO membrane and (C) GR/GO@PEI composite membrane. (D) Dynamic changes in wettability for various targeting membranes (note: M-1, the upper side of the GR membrane; M-2, the lower side of the GR membrane; M-3, the upper side of the GR/GO membrane; M-4, the lower side of the GR/GO membrane; M-5, the upper side of the GR/GO@PEI composite membrane; and M-6, the lower side of the GR/GO@PEI composite membrane). (E) The zeta potentials of the upper side (blue) and the lower side (red) of the GR/GO@PEI composite membranes in different pH environments (inset: a schematic illustration of the structure of the GR/GO@PEI composite membranes). (F) Raman spectra of the upper and lower sides of the GR/GO@PEI composite membranes. (G) XPS spectra of the GR membrane, GO membrane, the upper side as well as the lower side of the GR/GO membrane, and the GR/GO@PEI composite membrane. (H) The C, O and N element content values of different membranes. (I) XPS depth analysis results of the GR/GO@PEI composite membrane (note: blue: N element content from PEI, red: Si element content from the wafer substrate).

were due to the abundant polar oxygenated functional groups in GO. However, the zeta potential of the GR/GO@PEI composite membrane (Fig. 3E) increased to about 30 ± 3 mV even when it was placed in different pH environments. Moreover, there was little difference between the two sides of the GR/GO@PEI composite membrane. These results further indicate that PEI was a molecular bridge to form a cross-linked network with the GR/GO nanosheets.

Raman spectra measurement provided additional insight into the structure of the GR/GO@PEI composite membrane. As shown in Fig. 3F and S13,† each membrane manifested the typical characteristic peaks of D (at 1352 cm^{-1}) and G (at 1593 cm^{-1}) bands, which were representative to the defect degree and the ordered structure of graphene, respectively.[26] In addition, there was an obvious difference between the two sides of the GR/GO@PEI composite membrane for the intensity ratio (I_D/I_G), which reflected the average size of sp^2-dominated graphene and its corresponding defect extent. IR measurements were carried out to further study the covalent force of the GR/GO@PEI composite membrane. As shown in Fig. S14,† the characteristic absorption bands of GO and the GR/GO@PEI composite membrane can be seen at 3000–3400 cm^{-1} (O–H bond). Compared with the IR spectrum of pure GR and GO, the peak intensities of the GR/GO@PEI composite membrane at 2923 cm^{-1} and 2832 cm^{-1}, which corresponds to the C–H stretching vibrations of PEI, substantially increased. Furthermore, there were two bands at 1556 cm^{-1} and 1442 cm^{-1}, which can certify the presence of imide groups (O=C–N–C=O) in this composite membrane.[45] These characteristic absorption peaks have certified that PEI has modified the GR/GO sheets.

XPS was further applied to characterize the change in chemical composition of different membranes. As shown in Fig. 3G, C 1s (298 eV) and O 1s (540 eV) peaks appeared for all the investigated samples. Whereas, for both sides of the GR/GO@PEI composite membrane, new peaks associated with N 1s at 402 eV were observed (Fig. 3G and S15†). It was noted that the C/O mass ratio of the upper side of the GR/GO membrane and the GR/GO@PEI composite membrane was higher than that of the lower side of the GR/GO membrane and the GR/GO@PEI composite membrane, respectively. Moreover, there was a clear difference in the N content between the upper and the lower sides of the GR/GO@PEI composite membrane, which may be due to the different cross-linking degree of PEI (Fig. 3H). XPS depth analysis was further performed to distinguish the contents of N elements in the GR/GO@PEI composite membrane and Si elements (from the wafer substrate) varying with cross-sectional depth. The transition region with N content at 900–1200 s (about 80–110 nm) further demonstrated that PEI assumed the role of molecular bridge for the GR/GO membrane (Fig. 3I). XRD patterns of the GR/GO and GR/GO@PEI composite membranes in dry and wet states were tested. As shown in Fig. S16,† the interlayer spacing of the GR/GO membrane expanded from 0.85 ($2\theta = 10.26°$) nm to 1.27 nm ($2\theta = 7.6°$) after wetting with water. After modification with PEI, there were wide peaks at $2\theta = 17.71$–$26.61°$, corresponding to an interlayer spacing of 0.33–0.51 nm. Furthermore, there was almost no obvious change in the interlayer spacing of the GR/GO@PEI composite membrane after it was immersed in water. The stable interlayer spacing will facilitate the rejection of dye molecules.

3.3 Membrane permeability and selectivity properties

To explore the water permeation and dye molecule retention performance of the GR/GO@PEI composite membrane, a homemade cross-flow filtration apparatus was set up as shown in Fig. S17.† Firstly, GR/GO@PEI composite membranes with various molecular weights of PEI (PEI_{600}, PEI_{1800}, PEI_{10000}, PEI_{70000}) were fabricated to gain maximum penetration throughput with excellent rejection performance for separating the CR solution. As displayed in Fig. S18A,† the separation flux of the GR/GO@PEI composite membrane reached a maximum when PEI was at a suitable molecular weight. The lower molecular weight increased the relative crosslinking density at a unit molar amount, whereas the higher molecular weight brought about excessive steric hindrance, which resulted in a sharp reduction in the flux.[46] It was known that an ideal separation membrane with a thinner separation layer is beneficial for enhancing the permeation flux during the purification process.[6] Therefore, we further investigated the influence of the layer of the GR/GO@PEI_{1800} composite membrane and the concentration of the GO solution on the separation performance. It was concluded that the larger interface thickness was not conducive to an improvement in membrane separation flux (Fig. S18B†).

In addition, the GR/GO@PEI_{1800} composite membrane has excellent permeability and selectivity properties by controlling the concentration of the GO solution (Fig. S18C†). The water and dye molecule permeabilities of the GR/GO@PEI_{1800} composite membrane were further explored. As shown in Fig. 4A, B and S19,† the GR/GO@PEI_{1800} composite membrane exhibited an excellent rejection performance for various anionic dye molecules, such as EB (960.8 g mol^{-1}, 99.9% ± 0.5%), MB (799.8 g mol^{-1}, 99.8% ± 0.7%), CR (696.6 g mol^{-1}, 99.9% ± 0.3%), EBT (461.3 g mol^{-1}, 92.9% ± 2.5%), CSS (404.4 g mol^{-1}, 82.2% ± 1.1%). However, it displayed low rejection performance for MO (327.3 g mol^{-1}, 31.5% ± 1.9%). Therefore, the GR/GO@PEI_{1800} composite membrane can be used for the gating of anionic dye molecules with different molecular weights. As to cationic dye molecules, the GR/GO@PEI_{1800} composite membrane presented good rejection ability for VBB (506.08 g mol^{-1}, 78% ± 2.5%). However, it showed low rejection performance for Rh. B (479.01 g mol^{-1}, 45.2% ± 3.8%), MV (407.99 g mol^{-1}, 15.3% ± 2.8%) and DMPD (209.12 g mol^{-1}, 3.2% ± 0.8%) (Fig. S20†). Therefore, it can be inferred that the GR/GO@PEI_{1800} composite membrane showed excellent retention capacity for anionic dyes with a molecular weight above 400 g mol^{-1} and cationic dyes with a molecular weight above 500 g mol^{-1}. Furthermore, the permeability flux of pure water and CR reached 254 L m^{-2} h^{-1} bar^{-1} and 191 L m^{-2} h^{-1} bar^{-1}, respectively, which surpassed the majority of the previously reported separation membranes with similar rejection properties (Fig. 4C, Tables S1 and S2†). The rejection of the dye molecules was attributed to the collective effect of size

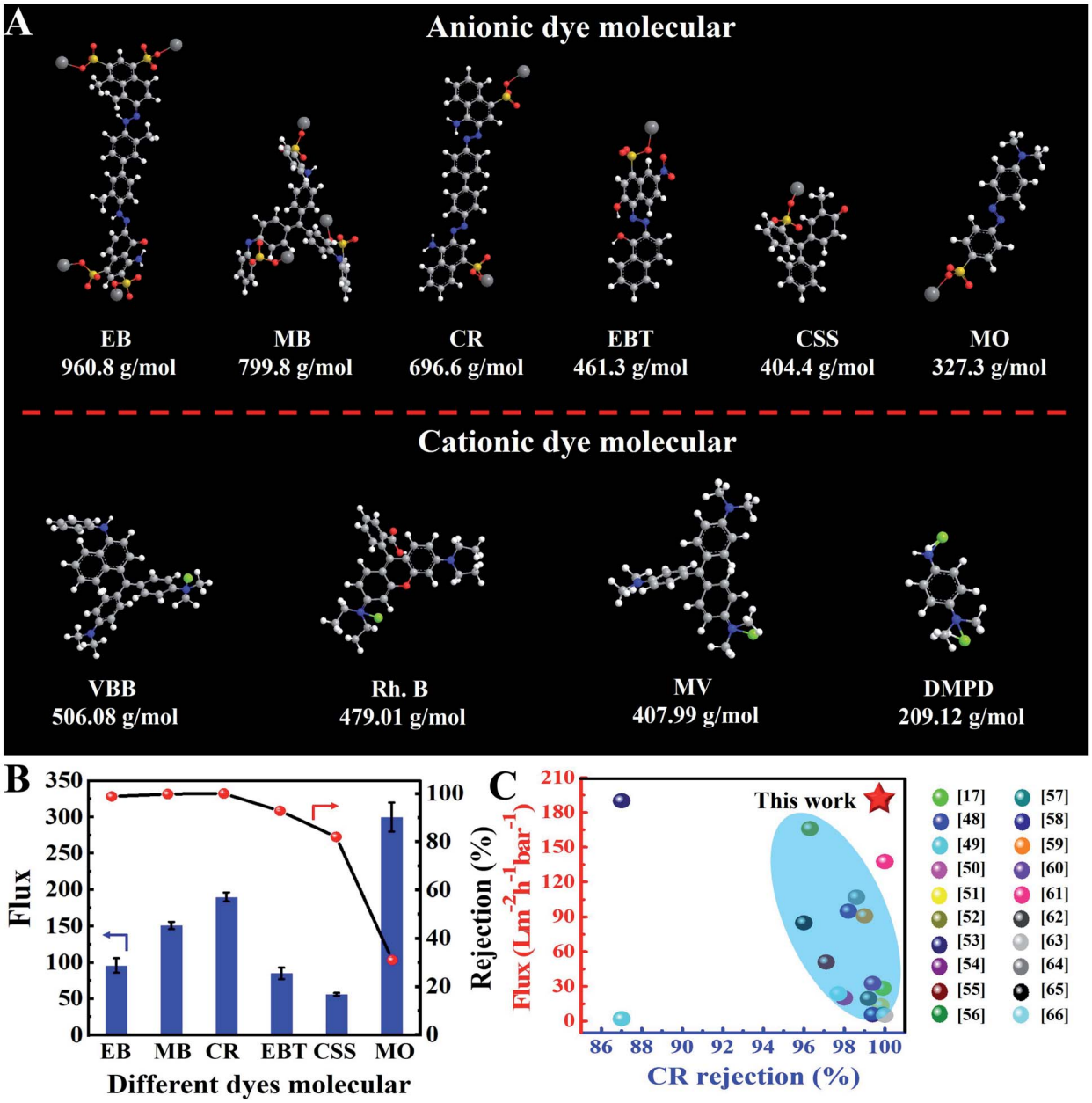

Fig. 4 (A) Ball and stick structures of different dye molecules. (B) The separation performances of the GR/GO@PEI$_{1800}$ composite membranes for various anionic dye aqueous solutions with different molecular weights (note: the unit of flux is L m^{-2} h^{-1} bar^{-1}). (C) A comparison of the separation performances of different membranes in the literature with this work.

screening and Donnan balance.[47] The separation mechanism of this composite membrane for various dyes is shown in Fig. S21.†

The physics and chemistry of a filtration membrane are major barriers for further practical applications. The mechanical stability of the GR/GO@PEI composite membrane was further evaluated. As shown in Fig. S22,† the GR/GO@PEI composite membrane was flexible enough to withstand several episodes of bending, and still maintained its complete crack-free structure (Movie S7†). Moreover, the GR/GO@PEI composite membrane was tightly bonded with the PVDF substrate. It was difficult to rub off from the substance after immersion in water compared with the GR/GO membrane (Fig. 5A, B and Movie S8†). These results demonstrated that the hydrophilic PEI served as a polymer chain bridge to form a network of covalent interlocked GR/GO sheets, which drastically enhanced the interactions within the GR/GO laminate. Furthermore, the chemical durability of the GR/GO@PEI$_{1800}$ composite membrane was evaluated by monitoring the microstructure after immersion in acidic water solution (1 mol L^{-1}), and alkaline solution (1 mol L^{-1}) for 72 h. As shown in Fig. 5C and D, the GR/GO@PEI$_{1800}$ composite membrane maintained its original micro-nanostructure toward these extreme environments. In addition, the GR/GO@PEI$_{1800}$ composite

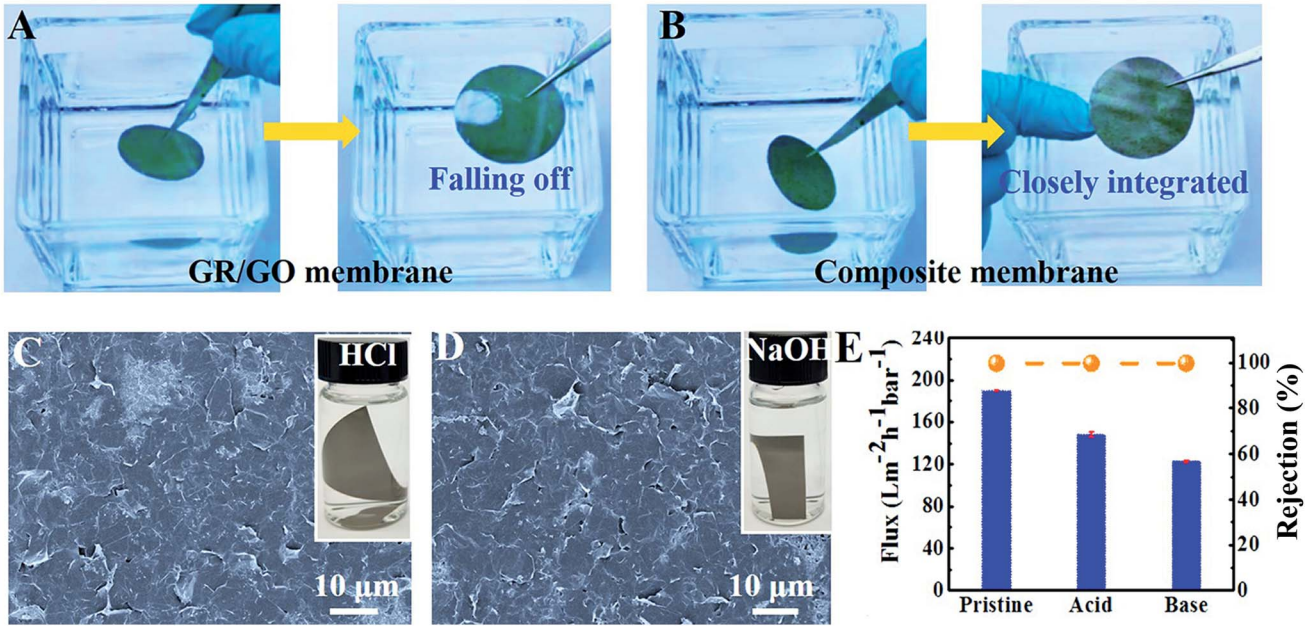

Fig. 5 Photographs of (A) the GR/GO membrane and (B) the GR/GO@PEI composite membrane being immersed in water and then rubbed, respectively. (C and D) SEM images of the GR/GO@PEI composite membrane after treatment in HCl (1 mol L^{-1}) or NaOH (1 mol L^{-1}) for 72 hours. (E) The separation flux and rejection ability of the GR/GO@PEI composite membrane for CR solution after treatment with HCl or NaOH for 3 days.

membrane still retained its high rejection performance with up to 99.9% ± 1.2% toward CR solution despite a slight drop in the separation flux (Fig. 5E). These results proved that the GR/GO@PEI_{1800} composite membrane has an excellent anti-corrosion property, which was beneficial for separating various dye molecules when treating actual wastewater. The

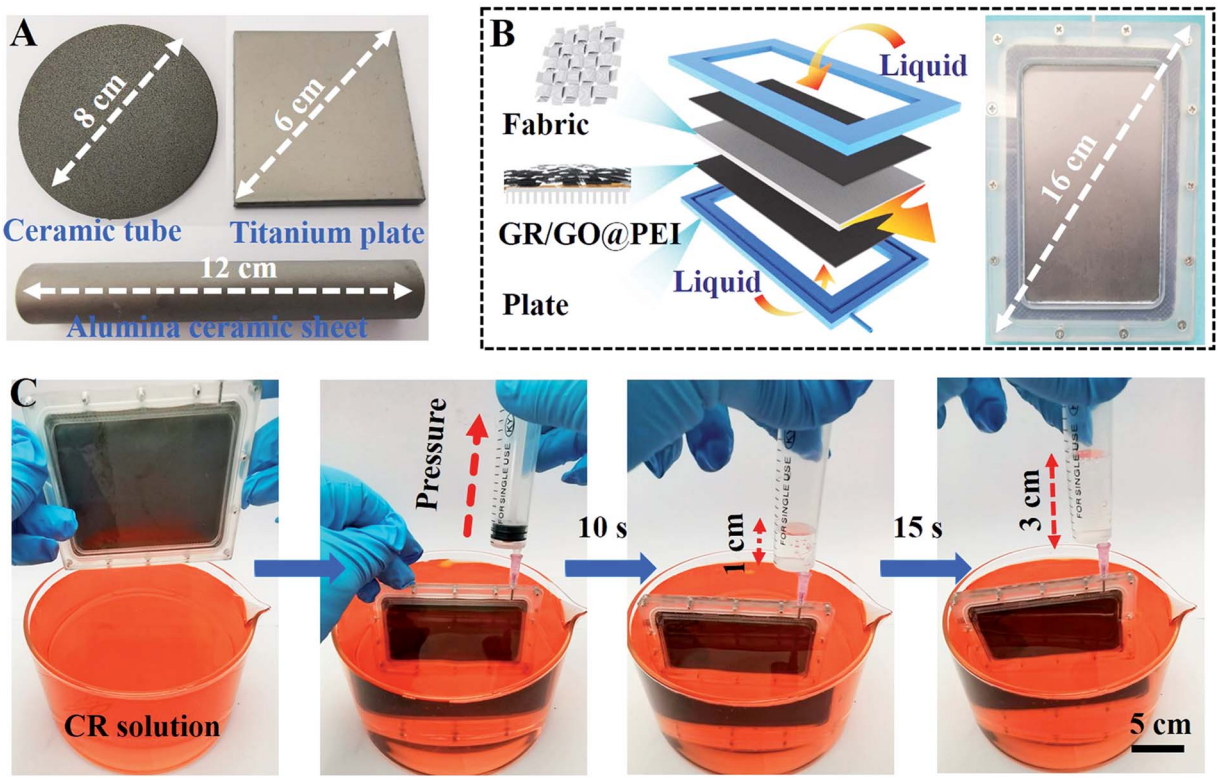

Fig. 6 (A) Photographs of the GR/GO@PEI_{1800} composite membrane transferred onto different filter substrates, including ceramic tubes, titanium plates and alumina ceramic sheets. (B) Photographs of the GR/GO@PEI_{1800} composite membrane serving as a separation module and its retention performance for CR solution with a concentration of 50 mg L^{-1} (C).

long-term stability of the GR/GO@PEI$_{1800}$ composite membrane was further evaluated. As shown in Fig. S23,† after separation for 23 hours, the GR/GO@PEI$_{1800}$ composite membrane still retained its high rejection performance with up to 99.9% ± 0.6% toward CR solution despite a slight drop in the separation flux. This result proved that the GR/GO@PEI$_{1800}$ composite membrane has excellent stability, which was beneficial for separating various dye molecules when treating actual wastewater.

Scale up is another key indicator for the further implementation of the GR/GO@PEI$_{1800}$ composite membrane. Excitingly, the GR/GO@PEI$_{1800}$ composite membrane can be transferred to any filter substrate despite its shape, specification or roughness (Fig. 6A). On this basis, we have successfully designed a water purification module by using the GR/GO@PEI$_{1800}$ separation membrane as a core formation (Fig. 6B). As shown in Fig. 6C and S24,† it can achieve high separation efficiency for CR (99.2 ± 1.5%) and EBT (92.9% ± 2.5%) solutions (Movies S9 and S10†). In order to simulate the actual sewage treatment process, we further set up a membrane purification device with a GR/GO@PEI$_{1800}$ composite membrane as a core separation layer (Fig. S25 and S26†). As shown in Fig. S25,† under a given pressure, this device can achieve high separation efficiency for a complex multi-component domestic sewage system, including EB, CR, MB, EBT and sludge (Movie S11†).

4. Conclusions

In summary, we have presented a facile, ultrafast, and environmentally friendly strategy for the construction of a GR/GO@PEI composite membrane on a large scale. The PEI molecule acted as an interfacial long-chain bridge to interlock the GR/GO laminate through covalent reactions. Therefore, the GR/GO@PEI composite membrane presents high mechanical stability and can be transferred to any substance, regardless of its shape, size, or chemical composition. Furthermore, this composite membrane has shown ultrafast molecular screening, with a maximum flux of up to 191 L m^{-2} h^{-1} bar^{-1} for CR solution and a rejection efficiency above 99.9%, exceeding the majority of previously reported GO-based separation membranes. Importantly, the GR/GO@PEI composite membrane exhibited excellent environmental stability and can realize the purification of actual, complex, multi-component, domestic sewage. This work has given overall consideration to large-scale, high separation flux and rejection capacity, stability, and practicality, showing potential applications for task-oriented wastewater treatment.

Conflicts of interest

There are no conflicts to declare.

Acknowledgements

This work was financially supported by the National Key Research and Development Program of China (2019YFC1606600, 2019YFC1606603), the K. C. Wong Education Foundation (GJTD-2019-13), Open Research Fund of Key Laboratory of Marine Materials and Related Technologies (2013DP173296), Ningbo Science and Technology Bureau (2018A610097), and the Bureau of Frontier Science and Education of the Chinese Academy of Sciences (QYZDB-SSW-SLH036).

Notes and references

1 Y. Kang, Y. Xia, H. T. Wang and X. W. Zhang, *Adv. Funct. Mater.*, 2019, **29**, 1902014.
2 J. T. Liu, D. Hua, Y. Zhang, S. Japip and T. S. Chung, *Adv. Mater.*, 2018, **30**, 1705933.
3 S. P. Surwade, S. N. Smirnov, I. V. Vlassiouk, R. R. Unocic, G. M. Veith, S. Dai and S. M. Mahurin, *Nat. Nanotechnol.*, 2015, **10**, 459–464.
4 Y. Zhao, Y. Li, J. J. Zhu, A. L. Larranag, S. S. Yuan, E. Orteg, J. N. Shen, C. Gao and B. V. Bruggen, *J. Mater. Chem. A*, 2019, **7**, 13903–13909.
5 C. X. Wang, C. X. Li, E. R. C. Rutledge, S. Che, J. Lee, A. J. Kalin, C. L. Zhang, H. C. Zhou, Z. H. Guo and L. Fang, *J. Mater. Chem. A*, 2020, **8**, 15891–15899.
6 M. C. Zhang, Y. Y. Mao, G. Z. Liu, G. P Liu, Y. Q. Fan and W. Q. Jin, *Angew. Chem., Int. Ed.*, 2020, **59**, 1689–1695.
7 Z. Y. Wang, Z. X. Wang, S. H. Lin, H. L. Jin, S. J. Gao, Y. Z. Zhu and J. Jin, *Nat. Commun.*, 2018, **9**, 2004.
8 Z. G. Peng, J. L. Gong, G. M. Zeng, B. Song, W. C. Cao, H. Y. Liu, S. Y. Huan and P. Peng, *J. Membr. Sci.*, 2019, **574**, 112–123.
9 R. Jin, P. Ting, Y. Y. Wu, C. Q. Chu, P. Cui, P. P. Zhang, X. Y. Ai, C. F. Fu, Z. J Yang and T. W. Xu, *Angew. Chem., Int. Ed.*, 2019, **58**, 16463–16468.
10 Y. J. Wang, L. B. Li, Y. Y. Wei, J. Xue, H. Chen, L. Ding, J. Caro and H. H. Wan, *Angew. Chem., Int. Ed.*, 2017, **56**, 8974–8980.
11 Y. Y. Fan, L. Y. Wei, X. X. Meng, W. M. Zhang, N. T. Yang, Y. Jin, X. B. Wang, M. W. Zhao and S. M. Liu, *J. Membr. Sci.*, 2019, **569**, 117–123.
12 J. Shen, G. Z. Liu, Y. F. Ji, Q. Liu, L. Cheng, K. C. Guan, M. C. Zhang, G. P Liu, J. Xiong, J. Yang and W. Q. Jin, *Adv. Funct. Mater.*, 2018, **28**, 1801511.
13 H. Li, T. J. Ko, M. Lee, H. S. Chung, S. S. Han, K. H. Oh, A. Sadmani, H. Kang and Y. W. Jung, *Nano Lett.*, 2019, **19**, 5194–5204.
14 X. L. Cui, X. L. Wu, J. Zhang, J. T. Wang, H. Q. Zhang, F. G. Du, L. B. Qu, X. Z. Cao and P. Zhang, *J. Mater. Chem. A*, 2019, **7**, 12698–12705.
15 H. Yang, L. X. Yang, H. J. Wang, Z. A. Xu, Y. M. Zhao, Y. Luo, N. Nasir, Y. M. Song, H. Wu, F. S. Pan and Z. Y. Jiang, *Nat. Commun.*, 2019, **10**, 2101.
16 K. Dey, S. Kunjattu H., A. M. Chahande and R. Banerjee, *Angew. Chem., Int. Ed.*, 2020, **59**, 1161–1165.
17 X. K. Zhang, H. Li, J. Wang, D. L. Peng, J. D. Liu and Y. T. Zhang, *J. Membr. Sci.*, 2019, **581**, 321–330.
18 S. Kandambeth, B. P. Biswal, H. D. Chaudhari, K. C. Rout, S. H. Kunjattu, S. Mitra, S. Karak, A. Das, R. Mukherjee, U. K. Kharul and R. Banerjee, *Adv. Mater.*, 2017, **29**, 1603945.

19 P. Z. Sun, K. L. Wang and H. W. Zhu, *Adv. Mater.*, 2016, **28**, 2287–2310.
20 H. Li, J. W. Hou, T. D. Bennett, J. D. Liu and Y. T. Zhang, *J. Mater. Chem. A*, 2019, **7**, 5811–5818.
21 L. D. Wang, M. S. H. Boutilier, P. R. Kidambi, D. J. Jang, N. G. Hadjiconstantinou and R. Karnik, *Nat. Nanotechnol.*, 2017, **12**, 509–522.
22 P. Z. Sun, M. Zhu, K. L. Wang, M. L. Zhong, J. Q. Wei, D. H. Wu, Z. P. Xu and H. W. Zhu, *ACS Nano*, 2013, **7**, 428–437.
23 B. X. Mi, *Science*, 2014, **343**, 740–742.
24 M. C. Zhang, K. C. Guan, Y. F. Ji, G. P. Liu, W. Q. Jin and N. P. Xu, *Nat. Commun.*, 2019, **10**, 1253.
25 J. C. Liu, L. J. Yu, G. C Yue, N. Wang, Z. M Cui, L. L. Hou, J. H. Li, Q. Z. Li, A. Karton, Q. F. Cheng, L. Jiang and Y. Zhao, *Adv. Funct. Mater.*, 2019, **29**, 1808501.
26 W. Y. Wang, C. C. Xie, L. Y. Zhu, B. J. Shan, C. N. Liu and F. Y. Cui, *J. Mater. Chem. A*, 2019, **7**, 172–187.
27 Y. B. Yang, X. D. Yang, L. Liang, Y. Y. Gao, H. Y. Cheng, X. M. Li, M. C. Zou, A. Y. Cao, R. Z. Ma, Q. Yuan and X. F. Duan, *Science*, 2019, **364**, 1057–1062.
28 S. Guo, Y. Nishina, A. Bianco and C. Mnard-Moyon, *Angew. Chem., Int. Ed.*, 2020, **59**, 1542–1547.
29 J. T. Wang, Z. J. Yuan, X. L. Wu, Y. F. Li, J. J. Chen and Z. Y. Jiang, *Adv. Funct. Mater.*, 2019, **29**, 1900819.
30 Y. J. Huang, W. T. Dou, F. G. Xu, H. B. Ru, Q. Y. Gong, D. Q. Wu, D. Y. Yan, H. Tian, X. P. He, Y. Y. Mai and X. L. Feng, *Angew. Chem., Int. Ed.*, 2018, **57**, 3366–3371.
31 G. Yang, Z. L. Xie, M. Cran, D. Ng, C. D. Easton, M. M. Ding, H. Xu and S. Gray, *J. Mater. Chem. A*, 2019, **7**, 19682–19690.
32 L. N. Nie, K. L. Goh, Y. Wang, J. Lee, Y. J. Huang, H. E. Karahan, K. Zhou, M. D. Guiver and T. H. Bae, *Sci. Adv.*, 2020, **6**, eaaz9184.
33 R. Y. Han and P. Y. Wu, *J. Mater. Chem. A*, 2019, **7**, 6475–6481.
34 S. F. Wang, D. Mahalingam, B. Sutisna and S. P. Nunes, *J. Mater. Chem. A*, 2019, **7**, 11673–11682.
35 X. Sui, Z. W. Yuan, C. Liu, L. Wei, M. Y. Xu, F. Liu, A. Montoya, K. Goh and Y. Chen, *J. Mater. Chem. A*, 2020, **8**, 9713–9725.
36 H. Y. Liu, H. T. Wang and X. W. Zhang, *Adv. Mater.*, 2015, **27**, 249–254.
37 M. C. Zhang, K. C. Guan, Y. F. Ji, G. P. Liu, W. Q. Jin and N. P. Xu, *Nature*, 2017, **550**, 380–383.
38 J. Zhong, W. Sun, Q. W. Wei, X. T. Qian and H. M. Cheng, *Nat. Commun.*, 2018, **9**, 3484.
39 Y. Liang, J. W. Shi, P. Xiao, J. He, F. Ni, J. W. Zhang, Y. J. Huang, C. F. Huang and T. Chen, *Chem. Commun.*, 2018, **54**, 12804–12807.
40 P. Xiao, J. C. Gu, C. J. Wan, S. Wang, J. He, J. W. Zhang, Y. J. Huang, S. W. Kuo and T. Chen, *Chem. Mater.*, 2016, **28**, 7125–7133.
41 X. Y. Wang, X. L. Yao and K. Müllen, *Sci. China: Chem.*, 2019, **62**, 1099–1144.
42 D. Parviz, S. Das, H. S. T. Ahmed, F. Irin, S. Bhattacharia and M. J. Green, *ACS Nano*, 2012, **6**, 8857–8867.
43 Z. J. Chen, A. Lohr, C. R. Saha-MÖller and F. WÜrthner, *Chem. Soc. Rev.*, 2009, **38**, 564–584.
44 J. J. Shao, W. Lv and Q. H. Yang, *Adv. Mater.*, 2014, **26**, 5586–5612.
45 C. Kim, S. Y. An, J. Lee, Q. Q. Zeng and J. D. Fortner, *ACS Appl. Mater. Interfaces*, 2019, **11**(1), 924–929.
46 J. J. Lu, Y. H. Gu, Y. Chen, X. Yan, Y. J. Guo and W. Z. Lang, *Sep. Purif. Technol.*, 2019, **210**, 737–745.
47 G. P. Liu and W. Q. Jin, *Sci. China Mater.*, 2018, **61**, 1021–1026.
48 P. Zhang, J. L. Gong, G. M. Zeng, C. H. Deng, H. C. Yang, H. Y. Liu and S. Y. Huan, *Chem. Eng. J.*, 2017, **322**, 657–666.
49 J. Q. Wang, P. Zhang, B. Liang, Y. X. Liu, T. Xu, L. F. Wang, B. Cao and K. Pan, *ACS Appl. Mater. Interfaces*, 2016, **8**, 6211–6218.
50 J. Ma, Y. He, G. Y. Zeng, F. Li, Y. B. Li, J. F. Xiao and S. Z. Yang, *Polym. Adv. Technol.*, 2018, **29**, 941–950.
51 J. Li, M. Y. Hu, H. C. Pei, X. H. Ma, F. Yan, D. S. Dlamini, Z. Y. Cui, B. Q. He, J. X. Li and H. Matsuyama, *J. Membr. Sci.*, 2020, **595**, 117547.
52 Z. Lin, Q. G. Zhang, Y. Qu, M. M. Chen, F. Soyekwo, C. X. Lin, A. M. Zhu and Q. L. Liu, *J. Mater. Chem. A*, 2017, **5**, 14819–14827.
53 A. Colomba, M. C. Biesinger, R. Divigalpitiya, F. A. Brandys and J. B. Gilroy, *Can. J. Chem.*, 2017, **95**, 1103–1109.
54 P. Li, Z. Wang, L. B. Yang, S. Zhao, P. Song and B. Khan, *J. Membr. Sci.*, 2018, **555**, 56–68.
55 S. Zhao and Z. Wang, *J. Membr. Sci.*, 2017, **524**, 214–224.
56 S. H. Zhou, Z. Xiong, F. Liu, H. B. Lin, J. Q. Wang, T. T. Li, Q. Han and Q. L. Fang, *J. Mater. Chem. A*, 2019, **7**, 632–638.
57 L. Wang, N. X. Wang, J. Li, J. W. Li, W. Q. Bian and S. L. Ji, *Sep. Purif. Technol.*, 2016, **160**, 123–131.
58 Q. Chen, P. P. Yu, W. Q. Huang, S. C. Yu, M. H. Liu and C. J. Gao, *J. Membr. Sci.*, 2015, **492**, 312–321.
59 W. Y. Shi, X. H. Zeng, H. B. Li, H. X. Zhang, X. H. Qin and R. Zhou, *J. Appl. Polym. Sci.*, 2020, **137**, 48569.
60 Q. Li, Z. P. Liao, X. F. Fang, J. Xia, L. H. Ni, D. P. Wang, J. W. Qi, X. Y. Sun, L. J. Wang and J. S. Li, *Desalination*, 2020, **479**, 114343.
61 W. M. Yu, Y. Liu, Y. C. Xu, R. J. Li, J. R. Chen, B. Q. Liao, L. G. Shen and H. J. Lin, *J. Membr. Sci.*, 2019, **581**, 401–412.
62 M. G. Buonomenna, L. C. Lopez, P. Favia, R. d'Agostino, A. Gordano and E. Drioli, *Water Res.*, 2007, **41**, 4309–4316.
63 H. W. Fan, J. H. Gu, H. Meng, A. Knebel and J. Caro, *Angew. Chem., Int. Ed.*, 2018, **57**, 4083–4087.
64 A. Asatekin, E. A. Olivetti and A. M. Mayes, *J. Membr. Sci.*, 2009, **332**, 6–12.
65 J. Guo, K. Y. Zhao, X. X. Zhang, Z. J. Cai, M. Chen, T. Chen and J. F. Wei, *Mater. Lett.*, 2015, **157**, 112–115.
66 H. P. Srivastava, G. Arthanareeswaran, N. Anantharaman and V. M. Starov, *Desalination*, 2011, **282**, 87–94.

